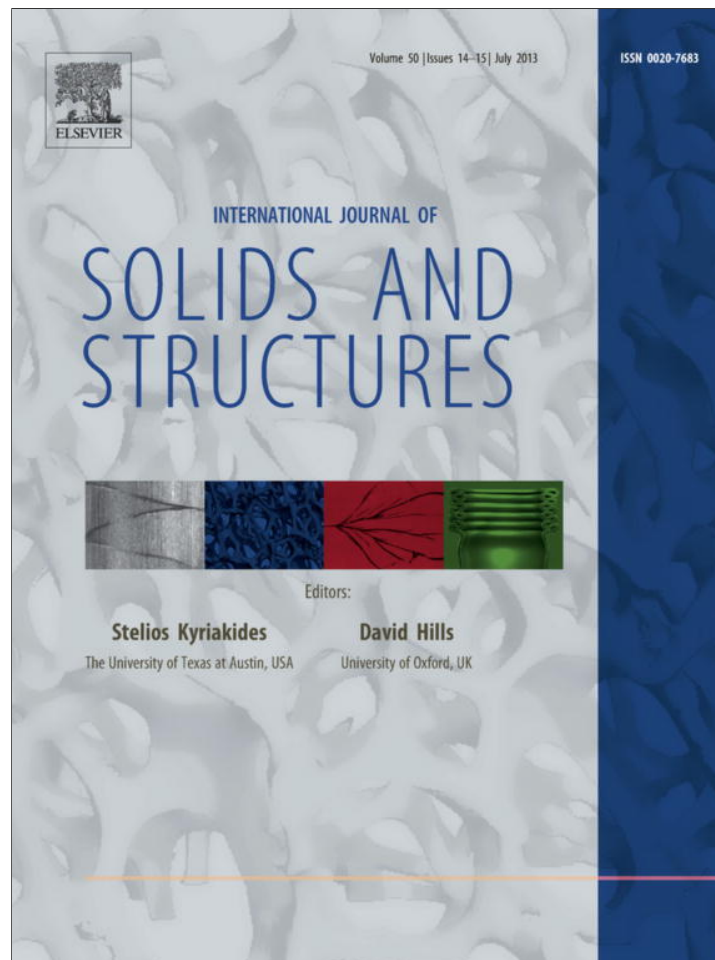


Provided for non-commercial research and education use.  
Not for reproduction, distribution or commercial use.



This article appeared in a journal published by Elsevier. The attached copy is furnished to the author for internal non-commercial research and education use, including for instruction at the authors institution and sharing with colleagues.

Other uses, including reproduction and distribution, or selling or licensing copies, or posting to personal, institutional or third party websites are prohibited.

In most cases authors are permitted to post their version of the article (e.g. in Word or Tex form) to their personal website or institutional repository. Authors requiring further information regarding Elsevier's archiving and manuscript policies are encouraged to visit:

<http://www.elsevier.com/authorsrights>



Contents lists available at SciVerse ScienceDirect

## International Journal of Solids and Structures

journal homepage: [www.elsevier.com/locate/ijsolstr](http://www.elsevier.com/locate/ijsolstr)

# Mechanism by which a frictionally confined rod loses stability under initial velocity and position perturbations

Tianxiang Su<sup>a</sup>, Nathan Wicks<sup>b</sup>, Jahir Pabon<sup>b</sup>, Katia Bertoldi<sup>a,c,\*</sup>

<sup>a</sup>School of Engineering and Applied Sciences, Harvard University, Cambridge, MA 02138, USA

<sup>b</sup>Schlumberger-Doll Research, One Hampshire Street, MD-B353, Cambridge, MA 02139, USA

<sup>c</sup>Kavli Institute for Bionano Science and Technology, Harvard University, Cambridge, MA 02138, USA

## ARTICLE INFO

### Article history:

Received 7 February 2013

Received in revised form 23 March 2013

Available online 11 April 2013

### Keywords:

Buckling

Instability

Friction

Confined elastic rods

## ABSTRACT

We present a theory to reveal for the first time the distinct mechanisms by which a compressed rod confined in a channel buckles in the presence of dry friction. Contrary to the case of a frictionless contact, with friction the system can bear substantially enhanced compressive load without buckling after its stiffness turns negative, and the onset of instability is strongly affected by the amount of perturbation set by the environment. Our theory, confirmed by simulations, shows that friction enhances stability by opening a wide stable zone in the perturbation space. Buckling is initiated when the applied compressive force is such that the boundary of the stable zone touches a point set by the environment, at a much higher critical load. Furthermore, our analysis shows that friction has a strong effect on the buckling mode; an increase in friction is found to lead to higher buckling modes.

© 2013 Elsevier Ltd. All rights reserved.

## 1. Introduction

Slender rods are ubiquitous in nature (Elbaum et al., 1996; Brangwynne et al., 2006; Senan et al., 2008), devices (Gansel et al., 2009; Wu et al., 2011; Su and Purohit, 2011) and engineering structures (Paslay and Bogy, 1964; Timoshenko and Gere, 1961; Wicks et al., 2008). At length scale separated by orders of magnitude, these one dimensional structures are typically constrained and mechanically supported: microtubules by the dense cellular matrix, plant roots by the surrounding soil and oilfield tubulars by the borehole walls. Despite the support, the rods can still buckle under large compressive forces, leading to catastrophic structural failure.

The mechanical stability of constrained rods has been studied for many years (Timoshenko and Gere, 1961; Lazopoulos, 1991; Domokos et al., 1997; Wicks et al., 2008), but surprisingly their buckling behavior is still often observed to deviate significantly from theories (Suryanarayana and McCann, 1994, 1995). For example, in the petroleum industry, horizontal wellbores are becoming more and more common. The buckling load of pipes that are used to perform operations in these horizontal wellbores is reported to be higher than the theoretical frictionless prediction by 30% to 50% (Gao and Miska, 2009, 2010; Mitchell, 2007). Moreover, noticeable hysteresis induced by buckling has been reported and the load required during unloading to unbuckle the rod has been found to be significantly lower than the buckling force (Suryanarayana and McCann, 1994,

1995). Although it has been suspected that these experimental observations are at least partly due to dry friction between the rod and the confinement, it is surprising that so far a theory capable of fully explaining them does not exist. Currently, it is not even clear whether friction just merely changes the dynamics of the system, or it completely alters the buckling mechanism.

To further illustrate the issue and to highlight the significant effect of friction, we start by presenting some dynamic simulation results, while leaving the details of the numerical analysis to be described later in Section 5. We simulate the compression-induced buckling of an elastic rod confined in a cylindrical channel to obtain the critical buckling load (see Fig. 1(A) and (B)). Both frictionless and frictional contact between the rod and the channel are considered, and the contributions of gravity, stretching, bending, twisting, shear, inertia and confinement of the rod are all taken into account. To trigger the instability, we introduce an imperfection in the form of an initial velocity perturbation. The perturbation is sinusoidal along the rod, with magnitude  $v_0$ , and it is applied in the transverse direction only at time  $t = 0$  s. In Fig. 1(D) we report the evolution of the reaction force in longitudinal direction as a function of the applied displacement for both frictionless and frictional cases under different initial velocity perturbation  $v_0$ . The reaction force under which the linear force–displacement relation breaks down is recorded as the critical buckling force. To clearly highlight the difference between frictional and frictionless situations, in Fig. 1(E) we report this critical force as a function of the perturbation magnitude  $v_0$ . Both Figs. 1(D) and (E) unambiguously reveal that in the case of frictionless contact, the

\* Corresponding author.

E-mail address: [bertoldi@seas.harvard.edu](mailto:bertoldi@seas.harvard.edu) (K. Bertoldi).

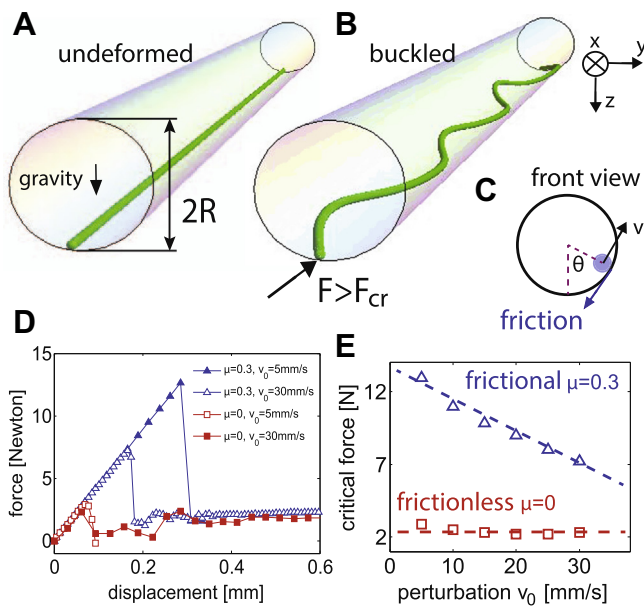


**Fig. 1.** (A) Undeformed and (B) deformed configurations of an elastic rod (length  $L = 3$  m, diameter  $d = 1.5$  mm, Young's modulus  $E = 77$  GPa) compressed in a  $R = 5.125$  mm horizontal cylindrical channel. The undeformed straight rod lies at the bottom of the channel because of gravity. To trigger instability in the dynamic simulations, an imperfection in the form of an initial velocity perturbation is applied in the transverse direction along the rod arc length  $s$  at time  $t = 0$  s:  $v = v_0 \sin(\omega^0 s)$ . Here  $\omega^0 = 6\pi/L$  is set according to the frictionless buckling mode (Paslay and Bogy, 1964; Wicks et al., 2008). (C): Cross-section view of the horizontal channel. The configuration of the deformed rod is characterized by the deflection angle  $\theta$ , which is a function of both the arc length  $s$  and the time  $t$ . (D) Under a displacement control, the rod is compressed and the reaction force is recorded in the simulations. This figure shows the force–displacement relation for four different cases: (red open squares) frictionless contact with  $v_0 = 5$  mm/s; (red close squares) frictionless contact with  $v_0 = 30$  mm/s; (blue open triangles) frictional contact with  $v_0 = 5$  mm/s; (blue close triangles) frictional contact with  $v_0 = 30$  mm/s. The force peak at which the linear force–displacement relation breaks down is recorded as the critical buckling force. (E) Numerically predicted critical buckling force as a function of the initial velocity perturbation amplitude  $v_0$ . Both frictionless (squares) and frictional (triangles) situations (friction coefficients  $\mu = 0, 0.3$ ) are shown (dashed lines are linear fits). Simulation details are provided in the Section 5. (For interpretation of the references to color in this figure legend, the reader is referred to the web version of this article.)

buckling load is independent of the magnitude of the initial perturbations, in agreement with the well-known frictionless theory (Paslay and Bogy, 1964). By contrast, for frictional contact the instability is shown not only to be initiated at a load much higher than that in the frictionless case, but also to depend on the magnitude of the perturbation  $v_0$ . We are not aware of any existing theory capable of explaining both the increase in buckling load and its strong dependence on the initial perturbation caused by friction. The main objective of this paper is therefore to develop a theory to unravel the mechanism by which a confined rod buckles in the presence of friction, with particular focus on the prediction of the onset of frictional buckling. This theory will provide an important tool both for researchers and industry, to fully understand the role played by friction and to precisely predict failure of structures in the presence of friction.

Most studies on buckling of confined rods ignore the effect of friction (Chen et al., 1990; Cunha, 2004; Domokos et al., 1997; van der Heijden et al., 2002), and are based on energy minimization methods. Straightforward introduction of dry friction within this framework leads to the paradoxical conclusion that buckling of a perfectly straight rod is essentially impossible if friction exists (Mitchell, 2007). In an attempt to overcome this issue, minimization of a generalized potential with a dissipative term has been proposed (Lazopoulos, 1991; Gao and Miska, 2009), but these stud-

ies fail in predicting the effect of imperfections on the buckling load. In a broader context, earlier attempts to incorporate dry friction in the stability analysis of elastic bodies also exist. However, these studies rely on a quasi-static assumption and interpret instability as existence of an equilibrium deformation path leading away from the probed state (Mróz and Plaut, 1991; Martinis and Raous, 2002; Nguyen, 2003, 2000). Therefore, they are unable to explain the dependency of stability on the perturbation revealed by the numerical simulations presented above.

The main contribution of this paper is not to provide a new mathematical formulation, rather, it is to use well-known equations to illustrate a poorly understood physical phenomenon, revealing how a frictionally confined rod buckles. In the absence of friction, the Kirchhoff analogy between the equilibrium of a uniform rod and the dynamics of a spinning top is well known (Kirchhoff, 1859). In particular, for the case of a frictionless rod confined in a channel the problem can be mapped to that of a heavy bead sliding on a rotating circle. With friction, however, the mapping is not obvious because the system is nonlinear and decomposing a continuous system with infinite degrees of freedom into a one-dimensional system is not straightforward. Therefore, additional assumptions have to be made and need to be justified. In this paper, we use detailed numerical simulations to determine such assumptions and show that at the onset of buckling only one deformation mode dominates. Only using this assumption can the problem of the frictional buckling of a rod be mapped to that of a sliding bead. Although the mathematical structure presented in this paper is not new (see the recent study of one-dimensional heavy bead (Burov, 2010) for example), and some features of the solution have been discussed (see Biemond et al., 2012 and the references therein), here we take a step forward and systematically study the behavior of the solutions, revealing for the first time how a frictionally confined rod buckles. In particular, an important feature not known before is the existence of a stable zone in the phase diagram that shrinks in response to an increase in compressive force. This finding helps in explaining why frictional buckling is not only initiated at a higher force but also strongly affected by perturbations. Our analysis reveals a frictional buckling mechanism that is distinct from the frictionless one and this has not been studied before. Furthermore, the investigation of buckling in a continuous system such as a rod requires understanding the interaction and evolution of different modes to determine the dominant one. Our study carefully addresses this important point, which is beyond the discussion in Burov (2010) and cannot be understood with a bead system.

In this paper, we present a theory that accounts for the non-equilibrium dynamics of the system and show that dry friction completely changes the mechanism by which a confined rod loses stability. The theory reveals that friction opens up a force-tunable stable zone not seen in the frictionless situation, and illustrates that instability of a frictional system will not be initiated when the system stiffness turns negative, rather, it will appear much later and is strongly affected by the perturbations. Furthermore, our analysis also shows that friction has a strong effect on the buckling mode; an increase in friction leads to a higher buckling mode. The theory suggests that stability of a frictional system depends on how perturbations are dissipated dynamically instead of quasi-statically, which cannot be revealed using an energy minimization method.

## 2. Dynamic equation of a confined rod

Let  $x$ – $y$ – $z$  defines a global coordinate system as shown in Fig. 1, with gravity acting in the  $z$  direction. We consider a horizontal cylindrical channel of radius  $R$ ,<sup>1</sup> aligned along the  $x$  direction. An

<sup>1</sup> To be exact and to account for the thickness of the rod,  $R$  here is the clearance, or  $R_{\text{channel}} - R_{\text{rod}}$ .

elastic rod of length  $L$  is confined in the channel, initially laying straight on the channel bottom due to gravity (Fig. 1(A)), so that the position of its center line is identified by:

$$\vec{r}_0 = [s, 0, -R], \quad (1)$$

with  $s$  denoting its arc length. With one end fixed, the other end of the rod is subjected to an axial compressive force  $F$  (Fig. 1(B)). We assume that the rod remains in contact with the channel and takes a deformed configuration:

$$\vec{r} = [x, R \sin \theta, -R \cos \theta], \quad (2)$$

where  $x = x(s, t)$  is the deformed axial coordinate and  $\theta = \theta(s, t)$  is the deflection angle with respect to the  $z$  direction (Fig. 1(C)). They are both functions of the arc length  $s$  and time  $t$ .

Unlike previous studies that assume quasi-staticity, we will investigate the dynamics of the rod. Therefore we start by building the Lagrangian of the system  $\mathcal{L}$ , which consists of the kinetic, bending, gravity and compressive force potentials. To the quadratic order in  $\theta$ ,  $\mathcal{L}$  can be written as

$$\mathcal{L} = \frac{1}{2} R^2 \left[ \rho \left( \frac{\partial \theta}{\partial t} \right)^2 - EI \left( \frac{\partial^2 \theta}{\partial s^2} \right)^2 - \frac{\rho g \theta^2}{R} + F \left( \frac{\partial \theta}{\partial s} \right)^2 \right], \quad (3)$$

with  $\rho$  being the mass density of the rod (per unit length),  $EI$  being the bending rigidity and  $g$  being the gravity constant. The corresponding Euler–Lagrange equation (without friction) for our system is obtained by minimizing  $\mathcal{L}$ :

$$\rho \frac{\partial^2 \theta}{\partial t^2} + EI \frac{\partial^4 \theta}{\partial s^4} + F \frac{\partial^2 \theta}{\partial s^2} + \frac{\rho g \theta}{R} = 0. \quad (4)$$

Eq. (4) governs the dynamics of a frictionless rod confined in a cylindrical channel in the  $\theta$  direction (i.e. direction that is normal to both the radial and axial directions of the channel). It can also be obtained by analyzing force balance of an infinitesimal segment of the confined rod in the  $\theta$  direction. A similar equation has been used to study the dynamic buckling and fragmentation of slender rods in the absence of friction (Gladden et al., 2005). However, since the goal of this work is to unravel the effect of friction on the buckling of a confined rod, we proceed by adding a nonlinear dry friction term to Eq. (4), which, as will be described soon, completely changes the mechanism by which a rod loses stability. In the presence of dry friction, the dynamic equation governing the response of the system becomes:

$$\rho \frac{\partial^2 \theta}{\partial t^2} + EI \frac{\partial^4 \theta}{\partial s^4} + F \frac{\partial^2 \theta}{\partial s^2} + \frac{\rho g \theta}{R} + \frac{F_{\text{friction}}(t, s)}{R} = 0, \quad (5)$$

where  $-F_{\text{friction}}(t, s) = -\text{sign}(\dot{\theta}) \mu N$  denotes the sliding dry friction force (per unit length), with  $\mu$  being the friction coefficient and  $N$  being the normal contact force between the rod and the horizontal channel. Note that Eq. (5) is valid only for (1) small  $\theta$ , which is sufficient for our goal of identifying the buckling onset, and (2) sliding friction where the magnitude of frictional force is exactly  $\mu N$ . We will point out the cases of sticking where  $|F_{\text{friction}}| \leq |\mu N|$  along our further analysis below. Furthermore, it is important to point out that several assumptions have been made in the derivation of Eq. (5). More specifically, we assumed that up to the onset of buckling (i) the normal contact force between the rod and the channel  $N = \rho g A$  is constant along the rod; (ii) the effect of twisting and shear of the rod is negligible; (iii) the axial compressive force in the rod is constant along the rod; (iv) the critical buckling mode is such that the rod remains in contact with the channel (as opposed to buckling vertically in the  $z$  direction against gravity, which would be energetically unfavorable). Moreover, later in this Section we will also assume that (v) at the onset of instability only one buckling mode dominates. The advantage of making all these assumptions is

that they lead to a simple analysis where the effect of friction on the buckling mechanism can be analytically investigated and clearly revealed. Furthermore, the validity of all these assumptions will be confirmed later in Section 5 by numerical simulations, where all these effects that are ignored by the theory will be taken into account.

The frictional term in Eq. (5) makes the equation nonlinear and difficult to analyze. To better investigate it, we first decompose  $\theta$  and  $\text{sign}(\dot{\theta})$  into Fourier series:

$$\begin{aligned} \theta(t, s) &= \sum A_n(t) \sin(\omega_n s), \\ \text{sign}(\dot{\theta}) &= \sum B_n(t) \sin(\omega_n s), \quad \text{with } \omega_n = \frac{n\pi}{L}, \end{aligned} \quad (6)$$

where, due to the nonlinearity of the sign function,  $B_n$  in general depends on  $\dot{A}_1, \dot{A}_2, \dots, \dot{A}_n, \dots$ :

$$B_n = \frac{2}{L} \int_0^L \text{sign} \left[ \sum_k \dot{A}_k \sin(\omega_k s) \right] \sin(\omega_n s) ds. \quad (7)$$

Substituting the two Fourier series into Eq. (5), we obtain the governing equations for the Fourier modes:

$$\ddot{A}_n + \frac{\omega_n^2}{\rho} \left( EI \omega_n^2 + \frac{\rho g}{R \omega_n^2} - F \right) A_n + \frac{\mu N B_n}{\rho R} = 0, \quad n = 1, 2, \dots, +\infty. \quad (8)$$

Eq. (8) is highly coupled because  $B_n$  depends on all  $A_k$ . However, as it has been mentioned above, when buckling occurs, only one deformation mode, let's say mode  $m$ , is expected to dominate, so that  $\theta(t, s) = A_m(t) \sin(\omega_m s)$  (no summation). Under this assumption, the Fourier coefficient  $B_m$  can be simplified as

$$\begin{aligned} B_m &\simeq \frac{2}{L} \int_0^L \text{sign}[\dot{A}_m \sin(\omega_m s)] \sin(\omega_m s) ds \\ &= \frac{2}{L} \int_0^L \text{sign}(\dot{A}_m) |\sin(\omega_m s)| ds = \frac{4}{\pi} \text{sign}(\dot{A}_m), \end{aligned} \quad (9)$$

which reveals that  $B_m$  only depends on  $A_m$ . By substituting Eq. (9) into Eq. (8), we obtain the decoupled equation governing the evolution of the dominant buckling mode  $A_m(t)$ :

$$\ddot{A}_m + \frac{\omega_m^2}{\rho} \left( EI \omega_m^2 + \frac{\rho g}{R \omega_m^2} - F \right) A_m + \text{sign}(\dot{A}_m) f = 0, \quad (10)$$

with  $f = 4\mu N / (\pi \rho R)$ . Therefore, to determine the onset of buckling, we look for conditions under which a single unstable mode with unbounded amplitude  $A_m(t)$  exists that satisfies Eq. (10). Note that the coefficient in front of  $A_m$  in the second term of Eq. (10):

$$k_m = \frac{\omega_m^2}{\rho} \left( EI \omega_m^2 + \frac{\rho g}{R \omega_m^2} - F \right) \quad (11)$$

is the square of the characteristic time frequency of the problem. In the absence of friction,  $k_m = 0$  corresponds to the onset of instability for the system. In fact, when  $f = 0$  (no friction) and  $k_m = 0$ , if the linearized system described by Eq. (10) is perturbed, there is no restoring force acting on it that brings it back to the equilibrium position. Therefore, periodic oscillation solutions whose magnitude is bounded by initial imperfection/perturbation cease to exist. However, we will see soon that these conclusions are not true anymore in the presence of dry friction ( $f > 0$ ). It is worth pointing out that Eq. (10) is identical to the dynamic equation for a frictional mass-spring system with an effective spring stiffness given by  $k_m$  in Eq. (11). Note that an increase in the compressive force  $F$  can turn the stiffness of the system  $k_m$  to negative. Finally, we note that our analysis so far assumes sliding friction. A stick state occurs when  $\dot{\theta} = 0$  (stationary) and  $\ddot{\theta} = 0$  (frictional force exactly balances other forces so there is no acceleration). Using Eq. (5), the latter condition reduces to:

$$\left| EI \frac{\partial^4 \theta}{\partial s^4} + F \frac{\partial^2 \theta}{\partial s^2} + \frac{\rho g \theta}{R} \right| = \left| \frac{F_{\text{friction}}}{R} \right| \leq \frac{\mu N}{R}. \quad (12)$$

In the Fourier space, these conditions for sticking are:

$$\dot{A}_m = 0, \quad |A_m| \leq \frac{f}{k_m}. \quad (13)$$

### 3. Instability analysis

To identify the onset of instability, we now look for the conditions under which an unbounded solution  $A_m(t)$  exists for Eq. (10). In particular, sketching its solution trajectories on the phase plane  $\dot{A}_m - A_m$  is a straightforward way to reveal instability. To fully unravel the effect of friction on the buckling of a constrained rod, six different conditions need to be discussed. Below we will first briefly discuss the three trivial frictionless cases ( $f = 0$ ), and then investigate the other three with friction ( $f > 0$ ).

#### 3.1. Frictionless contact

- **Case A:**  $f = 0, k_m > 0$ . In this case the solution to Eq. (10) is simply given by

$$A_m(t) = C_1 \sin(\sqrt{k_m}t) + C_2 \cos(\sqrt{k_m}t), \quad (14)$$

where  $C_1$  and  $C_2$  are two constants determined by the initial conditions. Therefore, if perturbed, the system will oscillate periodically with bound amplitude. Its trajectories on the plane  $\dot{A}_m - A_m$  are plotted in Fig. 2(A). In this case, we have only one stationary point  $[0, 0]$  on the phase plane, around which all trajectories circle. No unbound solution exists. Hence, as expected, the system is stable.

- **Case B:**  $f = 0, k_m = 0$ . In this case the solution to Eq. (10) becomes

$$A_m(t) = C_1 t + C_2 \quad (15)$$

and the trajectories are shown in Fig. 2(B). They all diverge and therefore the system is unstable to any perturbation away from the equilibrium  $[0, 0]$ . Hence,  $k_m = 0$  is an instability criterion, which, by using Eq. (11), leads to the critical force for mode  $m$ :

$$F_{m,cr}^0 = EI\omega_m^2 + \frac{\rho g}{R\omega_m^2}. \quad (16)$$

Here the superscript 0 stands for frictionless situation (i.e.  $\mu = 0$  and  $f = 0$ ). Since the buckling force for the system is the minimum force to trigger an unstable mode, in the frictionless situation we have:

$$F_{cr}^0 = \min_m F_{m,cr}^0 = 2\sqrt{\frac{\rho g EI}{R}}, \quad (17)$$

with a mode minimizer:

$$\omega^0 = \left(\frac{\rho g}{EI R}\right)^{1/4}. \quad (18)$$

Eqs. (17) and (18) are well known results and have previously been derived using the energy minimization method (Paslay and Bogy, 1964; Wicks et al., 2008). The dynamic approach we use here, however, can be extended to the frictional situations and will reveal a frictional buckling mechanism that the energy minimization methods are not able to show.

- **Case C:**  $f = 0, k_m < 0$ . For this last frictionless case, the solution to Eq. (10) is given by

$$A_m(t) = C_1 \cosh(\sqrt{-k_m}t) + C_2 \sinh(\sqrt{-k_m}t), \quad (19)$$

whose trajectories are shown in Fig. 2(C). Here, the stationary point  $[0, 0]$  is a saddle and the system remains unstable.

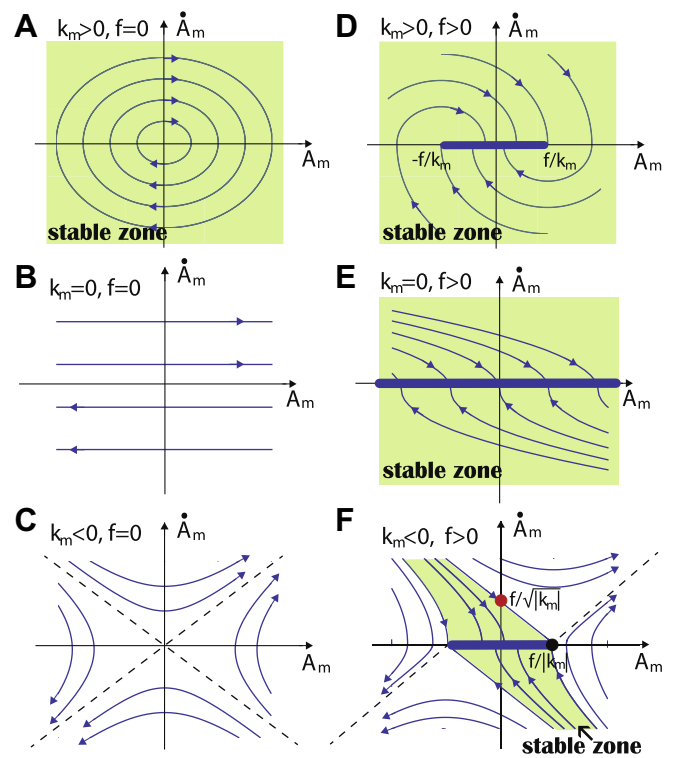


Fig. 2. Trajectories of the solutions of the dynamical system (Eq. (10)) on the phase plane  $\dot{A}_m - A_m$  for frictionless (A–C) and frictional (D–F) contacts. Trajectories that grow without bound correspond to an unstable situation. The green shadowed areas correspond to zones where the system is stable. For a frictionless system, stability only depends on the sign of the system stiffness  $k_m$ . For a frictional system, however, the system can be stable even when  $k_m < 0$  because friction opens a stable zone. In this case, stability depends strongly on perturbations.

All these observations fully agree with our knowledge of a frictionless system: buckling is initiated by any perturbation as the system stiffness  $k_m$  turns negative. However, in the case of frictional contact (i.e.  $f > 0$ ) these observations are no longer true.

#### 3.2. Frictional contact

- **Case D:**  $f > 0, k_m > 0$ . In this frictional case, the solution to Eq. (10) is given by:

$$A_m(t) + \text{sign}(\dot{A}_m) \frac{f}{k_m} = C_1 \sin(\sqrt{k_m}t) + C_2 \cos(\sqrt{k_m}t), \quad (20)$$

whose trajectories are plotted in Fig. 2(D). A comparison with the frictionless case shown in Fig. 2(A) reveals that the stationary point  $[0, 0]$  is now split and extended into a stationary line (thick line in Fig. 2(D)) defined by

$$A_m \in \left[-\frac{f}{k_m}, \frac{f}{k_m}\right], \quad \dot{A}_m = 0. \quad (21)$$

Every point on this stationary line corresponds to a “stick state” in which the external forces are not strong enough to move the rod against friction (i.e.  $|k_m A_m| < f$ , see Eq. (13) for sticking conditions). All trajectories on the phase plane are eventually dissipated onto this stationary line and the system is stable.

- **Case E:**  $f > 0, k_m = 0$ . In this case the solution to Eq. (10) is given by

$$A_m(t) = -\frac{1}{2} \text{sign}(\dot{A}_m) f t^2 + C_1 t + C_2, \quad (22)$$

whose trajectories are shown on Fig. 2(E). From Eq. (21), we can easily see that as  $k_m \rightarrow +0$ , the stationary line extends to  $A_m \rightarrow \pm\infty$ , onto which all trajectories are eventually dissipated. Therefore, in contrast with the frictionless situation, at  $k_m = 0$  no solution diverges (Fig. 2(E)). Hence, for a frictional system, loss of stiffness positivity does not lead to instability. This clearly demonstrates that the use of the frictionless theory in the buckling analysis will always underestimate the critical force.

- **Case F:**  $f > 0$ ,  $k_m < 0$ . This is a non-trivial case and represents the key result of this paper. When  $f > 0$  and  $k_m < 0$ , the analytic solution to Eq. (10) is given by

$$A_m(t) + \text{sign}(\dot{A}_m) \frac{f}{k_m} = C_1 \cosh(\sqrt{-k_m}t) + C_2 \sinh(\sqrt{-k_m}t), \quad (23)$$

with trajectories reported in Fig. 2(F). Remarkably, for this case a stable zone of finite size is created by dry friction, as shown by the colored green region in Fig. 2(F). Within this zone all trajectories are eventually dissipated onto the stationary line, while outside the zone all trajectories diverge. Therefore, a frictional system with  $k_m < 0$  can be stable or unstable, depending on the magnitude of the perturbation ( $A_m, \dot{A}_m$ ). Further inspection of Eq. (23) reveals that the stable zone is bounded by two hyperbolas and their linear asymptotes on the phase plane, all of which depend on the system stiffness  $k_m$  as

$$\begin{aligned} \left(A_m + \frac{f}{k_m}\right)^2 - \frac{\dot{A}_m^2}{|k_m|} &= \text{const}, \quad \dot{A}_m = -\sqrt{|k_m|} \left(A_m + \frac{f}{k_m}\right), \\ (\text{boundaries for } \dot{A}_m > 0), \\ \left(A_m - \frac{f}{k_m}\right)^2 - \frac{\dot{A}_m^2}{|k_m|} &= \text{const}, \quad \dot{A}_m = -\sqrt{|k_m|} \left(A_m - \frac{f}{k_m}\right). \\ (\text{boundaries for } \dot{A}_m < 0). \end{aligned} \quad (24)$$

Since  $k_m$  depends linearly on  $F$  (see Eq. (11)), Eq. (24) demonstrates that the boundaries, and therefore the size of the stable zone can be tuned by the external force  $F$ . When  $k_m = 0$  the stable zone covers the entire phase plane (Fig. 2(E)), whereas an increase in the compressive force will lead to a shrinkage of the stable zone towards  $[0, 0]$  (i.e. the stable zone reduces its size). Physically, this suggests that the tolerance of the rod to perturbations decreases as the applied compressive force increases. Moreover, since perturbation in reality is set by the environment and represented by a point (may not be stationary) on the phase plane, buckling of a frictional system is initiated when the applied compressive force is such that the boundary of the shrinking stable zone touches this point. We would like to remark that, to the best of our knowledge, this mechanism (distinct from the frictionless one) by which a frictionally confined rod loses stability has never been reported before.

The discussion above clearly highlights the fact that in the presence of friction,  $k_m = 0$  will not lead to instability (case E), and that when  $k_m < 0$ , the system can be either stable or unstable (case F). Hence, the zero stiffness criterion typically used to investigate the onset of frictionless instability is no longer suitable in the case of frictional contact. Contrary to the case of a frictionless contact, with friction the system can bear substantially enhanced compressive load without buckling after its stiffness turns negative, and the onset of instability is strongly affected by the amount of perturbation set by the environment.

It is worth pointing out here that the stable zone that opens for  $k_m < 0$  and  $f > 0$  can only be revealed when the non-equilibrium dynamic trajectories of a system are considered in the theory. In fact, the resultant force and inertia are not zero along most trajectories discussed above. This is the reason a minimum energy anal-

ysis, which always yields zero resultant force, is not capable of revealing the buckling mechanism in the presence of friction. Also, the quasi-static assumption commonly made in previous studies (Gao and Miska, 2009; Mróz and Plaut, 1991; Martinis and Raous, 2002; Nguyen, 2003, 2000) is not valid for the non-equilibrium trajectories shown on the phase plane. Furthermore, since friction splits a single stationary point into a line, there always exists a force-equilibrium path leading away from the trivial equilibrium  $[0, 0]$  (straight configuration). Claiming this as instability is incorrect, especially for the case with  $f > 0$  and  $k_m > 0$ .

#### 4. Special case: a rod laying on a flat plane

Before we discuss the results of dynamic simulations, we note that the analysis presented above can also be applied to the study of buckling of a compressed rod laying on a frictional two-dimensional plane, which is relevant to several applications including buckling of railroad tracks and of pipes on the sea floor (Miles and Calladine, 1999). In fact, this corresponds to the case of a rod confined in a channel of infinite radius (i.e.,  $R \rightarrow \infty$ ). For this special case, it is better to use the lateral deflection  $y$  instead of the deflection angle  $\theta$  in the analysis. Since  $y = R\theta$ , we can multiply Eq. (5) with  $R$  and obtain the dynamic equation for  $y$  as

$$\rho \frac{\partial^2 y}{\partial t^2} + EI \frac{\partial^4 y}{\partial s^4} + F \frac{\partial^2 y}{\partial s^2} + \frac{\rho g y}{R} + F_{\text{friction}}(t, s) = 0. \quad (25)$$

As  $R \rightarrow +\infty$ , the gravity term vanishes and the equation becomes

$$\rho \frac{\partial^2 y}{\partial t^2} + EI \frac{\partial^4 y}{\partial s^4} + F \frac{\partial^2 y}{\partial s^2} + F_{\text{friction}}(t, s) = 0. \quad (26)$$

The evolution equation for the unbound mode amplitude is obtained by performing Fourier transform on the above equation, yielding

$$\ddot{A}_m + \frac{\omega_m^2}{\rho} (EI\omega_m^2 - F)A_m + \text{sign}(\dot{A}_m)f = 0. \quad (27)$$

This equation has exactly the same mathematical structure as Eq. (10), and in this case

$$k_m = \frac{\omega_m^2}{\rho} (EI\omega_m^2 - F). \quad (28)$$

Therefore, everything about the stability of the system discussed above still holds. Setting  $k_m = 0$  and minimizing with respect to  $\omega_m$ , we obtain the well-known frictionless Euler buckling load  $F_{cr}^0 = EI\pi^2/L^2$  with the corresponding buckling mode  $\omega^0 = \pi/L$ . For a frictional contact, however, the onset of instability will be controlled by the perturbation as in the non-planar case in Section 3.

#### 5. Dynamic simulations

We next perform numerical analysis to compare with our theory. Following the approach that has been previously successfully applied to study the transient dynamics of drillstrings (Pabon et al., 2009, 2011), the rod is discretized and modeled as a chain of cylindrical rigid body segments held together through sets of axial, shear, torsion and bending springs. The spring constants are computed based on the material properties and the geometry of the segments (i.e., cross-sections and lengths) using standard Timoshenko beam theory (Timoshenko and Gere, 1961). Therefore, the axial and torsional stiffness between two adjacent segments ( $i$  and  $i + 1$ ) are given by<sup>2</sup>

<sup>2</sup> Note that the expressions for the bending and shear stiffness are more elaborate and not included here. We refer the readers to Timoshenko and Gere (1961) and Pabon et al. (2009) for more details.

$$K_{\text{axial}}^i = \left( \frac{l^i}{2E^i A^i} + \frac{l^{i+1}}{2E^{i+1} A^{i+1}} \right)^{-1}, \quad K_{\text{torsion}}^i = \left( \frac{l^i}{2G^i J^i} + \frac{l^{i+1}}{2G^{i+1} J^{i+1}} \right)^{-1}, \quad (29)$$

where  $l^i$ ,  $E^i$ ,  $A^i$ ,  $G^i$ , and  $J^i$  are the segment length, Young's modulus, cross section area, shear modulus and second moment of area of the segment  $i$  respectively. At any moment in time, the spring forces and moments are computed based on the spring constants and the displacements and rotations along the rod. The channel is modeled as a viscoelastic frictional contact using a modified Hertzian contact formulation that takes into account the compliance due to the hollow geometry of the rod cross-section (Budyans and Young, 2001; Pabon et al., 2009). Dry friction is implemented using Coulomb's law, which distinguishes between static and dynamic friction characterized by coefficients  $\mu_s$  and  $\mu_d$  respectively. Finally, a Newton–Raphson iteration scheme is used to integrate the equations of motion and update the rod configurations with computation time step  $dt = 1.6 \times 10^{-6}$  s.

In our simulations a rod of length  $L = 3$  m is considered, which is discretized and modeled as a chain of  $N = 500$  cylindrical segments. The rod has diameter  $d = 1.5$  mm, Young's modulus  $E = 77$  GPa and it is confined in a  $R = 5.125$  mm channel. For this system the frictionless theory predicts a critical load  $F_{\text{cr}}^0 = 2\sqrt{\rho g EI/R} = 1.3$  N with buckling wavenumber  $\omega^0 = 6\pi/L$  (Wicks et al., 2008).

As it has been discussed in the Introduction and shown in Fig. 1, we first simulate the compression of a confined elastic rod by fixing one end of the rod and compressing the other end with a constant velocity 1 mm/s. A series of simulations with frictionless and frictional contact, and with initial velocity perturbation of different magnitude  $v_0$  are performed. Force versus displacement curves are collected (Fig. 1(D)), and the force under which the linear force–displacement relation breaks down is recorded as the buckling force. As predicted by the theory, in the case of frictional contact the confined rod buckles at a much higher force compared to the frictionless situations, and the buckling force depends strongly on the initial perturbation (Fig. 1(E)). However, a quantitative comparison between this set of results and the theory is not possible, since the magnitude of both the perturbation and the applied force  $F$  (and therefore also the size of the stable zone) change as a function of time. In fact, during these simulations the compressive force increases as one keeps compressing the rod under displacement control. Moreover, the initial velocity perturbation decays in the presence of friction and no further perturbation is applied to the system at  $t > 0$  s.

To overcome the issue described above and quantitatively compare theory and numerical results, we perform another set of simulations where the rod is pre-compressed by a constant force  $F$  while keeping its ends fixed, so that the size of the stable zone does not change during the analysis. We denote the pre-compressive force as  $F = F_{\text{cr}}^0 + \Delta F$  with  $F_{\text{cr}}^0$  being the critical frictionless buckling force (Eq. (17)). Furthermore, a small initial transverse velocity perturbation  $v = v_0 \sin(\omega^0 s)$  is applied at  $t = 0$  s over the entire rod and the stability of the rod is tested for different combinations of  $\Delta F$  and  $v_0$ . The simulations run for 2 s and buckling, if it occurs, typically happens on a time scale of  $\sim 10$  ms. The results are shown in Fig. 3 where circular red markers correspond to stable straight configurations and black cross markers correspond to the buckled ones. In agreement with our expectations, when the contact is frictionless, the rod is stable for  $\Delta F < 0$ , but buckles for  $\Delta F > 0$  regardless of the initial perturbation  $v_0$  (Fig. 3(A)). By contrast, when friction is included by setting  $\mu = \mu_s = \mu_d = 0.3$ , stability is found to depend on  $v_0$ , just as our theory predicts (Fig. 3(B)). In fact, the rod is still stable under compressive force as high as 50 times the frictionless critical load, provided the perturbation is small.

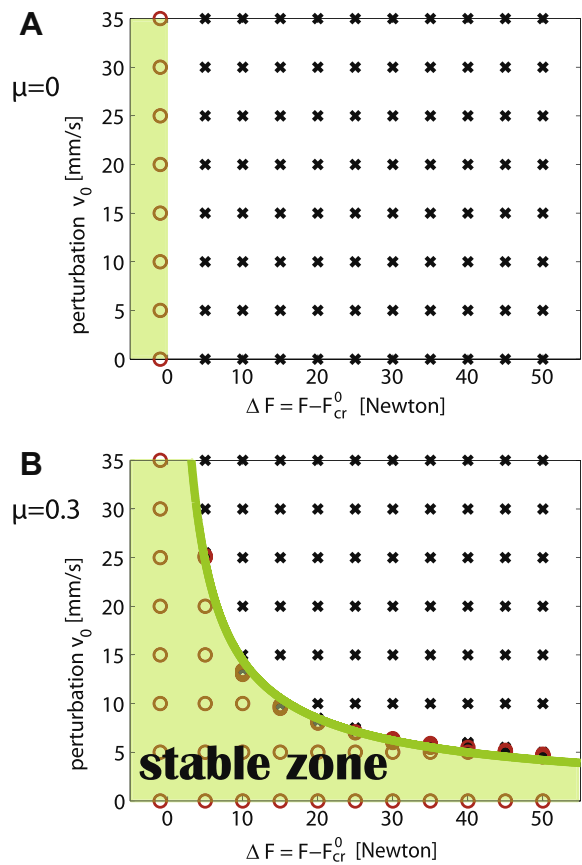
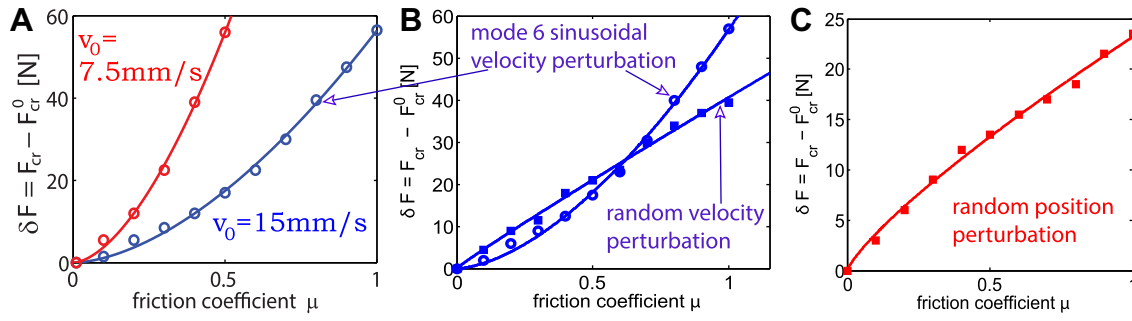


Fig. 3. Stability of a confined rod under different pre-compressive force  $F = F_{\text{cr}}^0 + \Delta F$  and velocity perturbation  $v_0$ . Circular red markers correspond to stable straight rods and black cross markers correspond to the buckled ones. Rods with (A) frictionless and (B) frictional ( $\mu = 0.3$ ) contacts with the channel are considered. (For interpretation of the references to color in this figure legend, the reader is referred to the web version of this article.)

This confirms that in the presence of friction, loss of stiffness positivity (i.e.  $\Delta F \geq 0$ ) does not lead to instability. Moreover, the numerical results are also found to be in quantitative agreement with the analytical predictions. Since Eq. (24) reveals that the stable zone in Fig. 2(F) intersects the  $\dot{A}_m$  axis at  $\pm f/\sqrt{|k_m|} \sim \Delta F^{-0.5}$ , one expects that the boundary between straight and buckled configurations in Fig. 3(B) follows a power law of  $-0.5$ . Fitting to the simulation results yields  $v_0 \sim \Delta F^{-0.77}$ , roughly in agreement with the theory.

We next fix the initial velocity perturbation and investigate the buckling force as a function of the friction coefficient  $\mu = \mu_s = \mu_d$ . We first perform two sets of simulations in which the initial velocity perturbation is set to be  $v = v_0 \sin(\omega^0 s)$ , with  $v_0 = 15$  mm/s and  $v_0 = 7.5$  mm/s respectively. This velocity perturbation is again applied only at  $t = 0$  s in the lateral direction. The buckling force as a function of  $\mu$  is plotted in Fig. 4(A). In particular, we plot the difference between the frictional and frictionless buckling force  $\delta F$  (i.e.  $\delta F = F_{\text{cr}} - F_{\text{cr}}^0$ ), so that when  $\mu = 0$ ,  $\delta F = 0$ . As expected, higher friction yields higher buckling force for a fixed perturbation magnitude, and decreasing the perturbation magnitude results in a higher buckling force for all  $\mu$ . Moreover, our theory predicts  $\delta F \sim \mu^2$  while simulations give a power law of 1.65 and 1.64 for  $v_0 = 15$  mm/s and  $v_0 = 7.5$  mm/s, respectively.

In the above two sets of simulations, the initial velocity perturbation is set as sinusoidal with the same wavenumber as the frictionless buckling mode ( $\omega = \omega^0 = 6\pi/L$ ). However, in reality the perturbation experienced by the system is random. To investigate



**Fig. 4.** Buckling force as a function of the friction coefficient  $\mu$ . (A) Simulations with an initial sinusoidal velocity perturbation of the form  $v = v_0 \sin(6\pi x/L)$ . Red and blue markers are for  $v_0 = 7.5$  and  $15$  mm/s respectively. Mode 6 is the frictionless buckling mode. (B) Simulations with a random initial velocity perturbation  $v \in [-15, 15]$  mm/s (solid blue squares). For comparison, we re-plot the results for the case of a sinusoidal perturbation of the same magnitude here (open blue circles). (C) Simulations with a random position perturbation. (For interpretation of the references to color in this figure legend, the reader is referred to the web version of this article.)

this important case we use the same simulation setup as described above, except that now at  $t = 0$  s we assign a random velocity  $v_0 \in [-15, 15]$  mm/s on each node along the rod in the lateral direction. In Fig. 4(B) we use square markers to report the buckling force in the form  $\delta F = F_{cr} - F_{cr}^0$  as a function of the friction coefficient  $\mu$ . For comparison, in the same plot we use circular markers to show the results for the case of a sinusoidal perturbation with the same magnitude,  $v_0 = 15$  mm/s. The two cases show similar buckling force when the friction coefficient is small. However, for  $\mu > 0.5$  the system with random perturbation shows significantly lower critical force, leading to a reduced power law  $\delta F \sim \mu^{0.95}$ . A similar trend is also found in simulations with random position perturbations (see Fig. 4(C)).<sup>3</sup> For this case, we find  $\delta F \sim \mu^{0.81}$ , while our theory predicts a power law of 1.0.

We then ask why random perturbation yields lower buckling force for large  $\mu$ . We start by noting that when deriving the power law from our theory we assume that the rod will buckle into the same mode  $m$  for all values of  $\mu$ . However, Fourier transforms of the simulation rod coordinates indicate that for the case of random perturbations the triggered buckling mode is not the same for all  $\mu$ . This can be clearly seen in Fig. 5(A) where we report the evolution of the buckling mode  $m$  as a function of the friction coefficient  $\mu$ . Interestingly, the buckling mode  $m$  is found to monotonically increase with  $\mu$ , ranging from 6 to 32 for the case of random velocity perturbation and from 6 to 21 for the case of random position perturbation. Moreover, it is important to note that the Fourier transforms of the rod coordinates reveal that in all the considered configurations a single modes dominates, confirming the validity of the assumption (v) made in the derivation of the theory.

To understand the observed increase in mode number as a function of friction, we inspect the size of the stability zones for different modes. This is determined by the  $x$ - and  $y$ -intercepts of the zone:  $A_{m,cr} = \pm f/|k_m|$  and  $\dot{A}_{m,cr} = \pm f/\sqrt{|k_m|}$  (see Fig. 2(E), black and red circular markers). In fact, these two quantities not only determine the stable zone size, but also are the critical initial velocity and position perturbations a system can tolerate without buckling. In particular,  $\dot{A}_{m,cr}$  and  $A_{m,cr}$  are given by

$$\dot{A}_{m,cr} = \frac{f}{\sqrt{|k_m|}} = \frac{f\sqrt{\rho}}{\omega_m \sqrt{F - F_{m,cr}^0}}, \quad A_{m,cr} = \frac{f}{|k_m|} = \frac{f\rho}{\omega_m^2 (F - F_{m,cr}^0)}, \quad (30)$$

<sup>3</sup> To apply random position perturbations, small random forces in the lateral direction of the rod are first applied on all nodes for 1 ms to obtain random position perturbation. The configurations are then taken as rod initial configurations to perform buckling tests with zero initial velocity.

with

$$F_{m,cr}^0 = EI\omega_m^2 + \frac{\rho g}{R\omega_m^2}, \quad \text{and} \quad f = \frac{4\mu N}{\pi\rho R}. \quad (31)$$

Here  $F_{m,cr}^0$  denotes the force required to trigger mode  $m$  when there is no friction. In Fig. 5(B) we plot  $\dot{A}_{m,cr}$  (representing the  $y$ -intercept of the stability zone for mode  $m$ ) as a function of the compressive force  $F$ , with different colors representing different wavenumber  $\omega_m$ . As expected,  $\dot{A}_{m,cr}$  decreases as the applied compressive force increases. More importantly, we find that the higher the wavenumber  $\omega_m$ , the faster  $\dot{A}_{m,cr}$  decreases, and so the faster the stable zone shrinks. This suggests that, in the case of a random velocity perturbation where all modes may be excited, a mode with wavenumber higher than the frictionless one can be triggered if its stability zones is the first to touch the point representing the system perturbation. We expect this more likely to occur at large  $\mu$ , where instability is triggered at a high compressive force. This observation is clearly confirmed by the numerical data (see Fig. 5(A)), which shows that the buckling mode  $m$  monotonically increases as a function of  $\mu$ . Finally, we note that modes with wavenumber smaller than  $\omega^0$  will never be triggered, since not only  $F_{cr,m}^0 > F_{cr}^0$ , but also their associate stable zones shrink at slower rates (Fig. 5(B)). Similar argument can be applied for the case of random position perturbation by investigating the evolution of  $A_{cr,m} = f/|k_m|$  as a function of applied compressive force for different modes. We note that in reality the rod will experience both position and velocity random perturbations. However, also in this case we expect both the critical force and critical mode to increase with  $\mu$ .

Finally, we used numerical simulations to confirm the validity of all the assumptions we made in the theory (see Section 2). (i) In all our simulations the normal contact force is found to be uniform along the rod before buckling occurs. This is true because up to the onset of buckling the rod is straight and lies on the bottom of the channel. In the post-buckling regime the normal contact force is found to be, as expected, a complicated function of the rod position. Since our theory is developed to identify the onset of frictional buckling but not to understand the post-buckling behavior, the constant normal force assumption is reasonable and sufficient. (ii) We monitor the torsional and shear energy in all our simulations and observe that their contribution is negligible compare to that of the bending and stretching energies. As an example, in Fig. 6(A) we report the evolution over time of the torsional,  $E_{tor}$ , and shear,  $E_{shear}$ , energies for a simulation where  $\mu = 0.3$ ,  $\Delta F = 5$  N and  $v_0 = 35$  mm/s (sinusoidal perturbation with wavenumber  $\omega^0$ ). The results clearly show that the torsional and shear energies of the rod during the simulation are indeed very small compared to total energy. (iii) In the simulations we find that the maximum variation of the axial compressive force along the rod is less than 7% of the frictionless buckling force  $F_{cr}^0$ . This confirms

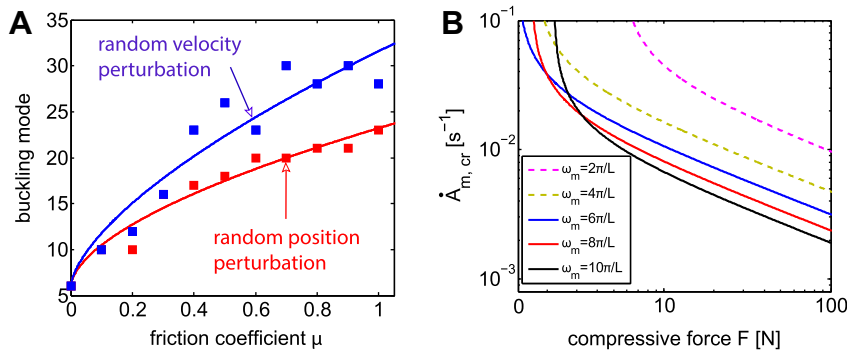


**Fig. 5.** (A) Buckling mode as a function of friction coefficient  $\mu$  for simulations with an initial random velocity perturbation (blue) and a random position perturbation (red). (B) Critical initial velocity perturbation  $\dot{A}_{m,cr}$  for different wavenumber  $\omega_m = m\pi/L$  as a function of the compressive force  $F$ . Green dashed, magenta dashed, blue solid, red solid and black solid curves for modes  $m = 2, 4, 6, 8, 10$  respectively. In particular, mode 6 is the frictionless buckling mode so it appears first as the compressive force increases. But it is the higher number modes that decrease faster. Therefore, at high compressive force, higher number modes have smaller buckling forces given the same velocity perturbation. For this reason, a frictional system does not necessarily buckle into the frictionless mode. (For interpretation of the references to color in this figure legend, the reader is referred to the web version of this article.)

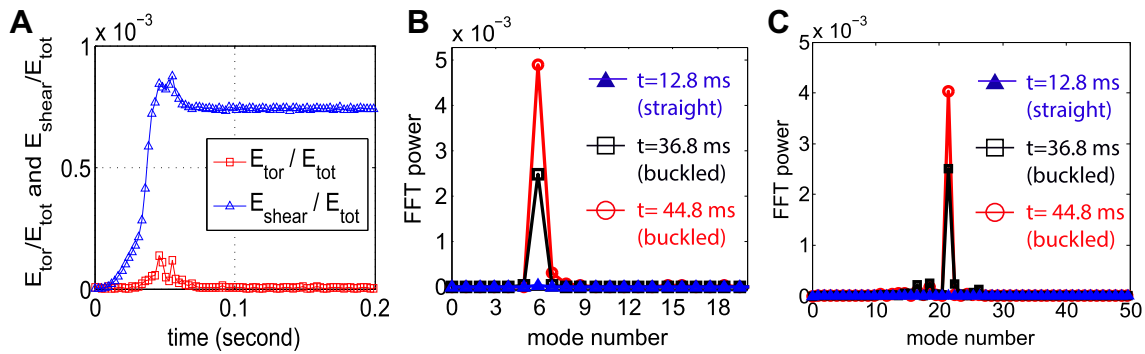


**Fig. 6.** (A)  $E_{tor}/E_{tot}$  (red squares) and  $E_{shear}/E_{tot}$  (blue triangles) as a function of time for a simulation where  $\mu = 0.3$ ,  $\Delta F = 5$  N and  $v_0 = 35$  mm/s (sinusoidal velocity perturbation with  $\omega^0 = 6\pi/L$ ). The data show that rod twisting and shear indeed can be ignored in the modeling, since their contribution to the total energy of the system is negligible. (B) Fourier transform power of the rod configurations for the same simulation. Blue triangles correspond to a configuration before buckling at  $t = 13$  ms. Black squares and red circles correspond to configurations after buckling at  $t = 37$  and  $45$  ms, respectively. (C) Fourier transform power of the rod configurations for a simulation with random initial position perturbation ( $\mu = 0.9$ ). The symbols have the same meanings as in Figure B. A single, but higher number mode  $m = 21$  is triggered in this case. (For interpretation of the references to color in this figure legend, the reader is referred to the web version of this article.)

that the assumption of a constant axial compressive force is valid. (iv) Buckling in the vertical direction (against gravity) is not seen in any of our simulations. This is expected, since the gravitational potential is linear in deformation while all other elastic energies are of second order. (v) Finally, to confirm that at the onset of buckling only one unstable mode dominates, we perform Fourier transform on the coordinates of the rod obtained numerically at different time steps and determine which mode (s) dominate at any time. In all the simulations we find that a single mode dominates. Typical results, for a case with a sinusoidal velocity perturbation with wavenumber  $\omega = \omega^0 = 6\pi/L$  and another case with a random position perturbation, are shown in Fig. 6(B) and (C), respectively. We note that for the sinusoidal perturbation, mode  $m = 6$  is the single dominant mode at the onset of buckling, while for the random perturbation, a single, but higher mode  $m = 21$  dominates. Hence, the simulations validate all the simplifications introduced in the theory.

## 6. Conclusions and discussion

In conclusion, our theory, confirmed by simulations, shows that dry friction changes the mechanism by which a confined rod buckles by opening a force-tunable stability zone in the perturbation space. With dry friction, the rod can tolerate substantial perturbation without buckling even after the system stiffness turns negative. Furthermore, friction strongly affects the buckling mode.

Modes higher than the frictionless buckling mode are triggered at high friction coefficients, while modes lower than the frictionless one can never be triggered. The physics behind this unusual instability mechanism is that dry friction is a strong dissipation mechanism. Its magnitude is a constant while other restoring forces are linear to either position or velocity. Therefore, in the neighborhood of the straight configuration, dissipation is a dominant effect. It is straightforward to show that if friction is of viscous type, being linear to the velocity, no stable zone will open up. Mathematically, the opening of a stable zone in the perturbation space is due to breaking of linearity by friction. For a linear system, it is well-known that no trajectory can be stable if one solution diverges on the phase plane (Jordan and Smith, 1999). However, friction introduces nonlinearity and splits a single stationary point into a line, leading to the co-existence of both stable and unstable trajectories on a phase plane. Future works will focus on characterizing the perturbation set by the environment and also extending the theory to understand the instability of other mechanical structures such as thin films and membranes in the presence of friction.

## Acknowledgments

We thank Dr. Pedro M. Reis and James Miller at Massachusetts Institute of Technology for helpful discussions. This research is funded by Schlumberger-Doll Research.

## References

- Biamond, J.J.B., van de Wouw, N., Nijmeijer, H., 2012. Bifurcations of equilibrium sets in mechanical systems with dry friction. *Physica D* 241, 1882–1894.
- Brangwynne, C.P., MacKintosh, F.C., Kumar, S., Geisse, N.A., Talbot, J., Mahadevan, L., Parker, K.K., Ingber, D.E., Weitz, D.A., 2006. Microtubules can bear enhanced compressive loads in living cells because of lateral reinforcement. *J. Cell Biol.* 173, 733–741.
- Budyans, R., Young, W., 2001. *Roark's Formulas for Stress & Strain*, seventh ed. McGraw-Hill Professional, ISBN 0070725411.
- Burov, A.A., 2010. On the bifurcations of relative equilibria of a heavy bead sliding with dry friction on a rotating circle. *Acta Mech.* 212, 349–354.
- Chen, Y., Lin, Y.H., Cheatham, J.B., 1990. Tubing and Casing Buckling in Horizontal Wells. *JPT* 42 (2), 140–143, 185.
- Cunha, J.C., 2004. Buckling of tubulars inside wellbores: a review on recent theoretical and experimental works. *SPE Drill Compl.* 19 (1), 13–19 (SPE-87895-PA).
- Domokos, G., Holmes, P., Royce, B., 1997. Constrained Euler buckling. *J. Nonlinear Sci.* 7, 281–314.
- Elbaum, M., Fygenson, D.K., Libchaber, A., 1996. Buckling microtubules in vesicles. *Phys. Rev. Lett.* 76, 4078–4081.
- Gao, G., Miska, S., 2009. Effects of boundary conditions and friction on static buckling of pipe in a horizontal well. *Soc. Petrol. Eng. J.* 14, 782.
- Gao, G., Miska, S., 2010. Effects of friction on post-buckling behavior and axial load transfer in a horizontal well. *Soc. Petrol. Eng. J.* 15 (4), 1104–1118 (SPE-120084-PA).
- Gansel, J.K., Thiel, M., Rill, M.S., Decker, M., Bade, K., Saile, V., Freymann, G.V., Linden, S., Wegener, M., 2009. Gold helix photonic metamaterial as broadband circular polarizer. *Science* 325, 1513–1515.
- Gladden, J.R., Handzy, N.Z., Belmonte, A., Villermaux, E., 2005. Dynamic buckling and fragmentation in brittle rods. *Phys. Rev. Lett.* 94, 035503.
- Jordan, D.W., Smith, P., 1999. *Nonlinear Ordinary Differential Equations. An introduction to Dynamical Systems*. Oxford University Press.
- Kirchhoff, G., 1859. Über das Gleichgewicht und die Bewegung eines unendlich dünnen elastischen stabes. *J. Math. (Crelle)* 56, 285–313.
- Lazopoulos, K.A., 1991. Column buckling under friction. *Arch. Appl. Mech.* 61, 215–221.
- Miles, D.J., Calladine, C.R., 1999. Lateral thermal buckling of pipelines on the sea bed. *J. Appl. Mech.* 66 (4), 891–897.
- Mitchell, R.F., 2007. The effect of friction on initial buckling of tubing and flowlines. *SPE Drill Compl.* 22 (2), 112–118 (SPE-99099-PA).
- Mróz, Z., Plaut, R.H., 1991. On the stability and post-critical behaviour of elastic structures with dry friction. *Int. J. Solids Struct.* 29, 1241.
- Martinis, J.A.C., Raous, M., 2002. *Friction and Instabilities*. Springer.
- Nguyen, Q.S., 2000. *Stability and Nonlinear Solid Mechanics*. Wiley, Chichester.
- Nguyen, Q.S., 2003. *Instability and friction*. *C.R. Mec.* 331, 99–112.
- Pabon, J., Wicks, N., Chang, Y., Dow, B., Harmer, R., 2009. Modeling transient vibrations while drilling using a finite rigid body approach. *First Int. Colloq. Nonlinear Dyn. Deep Drill. Syst.*, 83–87.
- Pabon, J., Wicks, N., Chang, Y., Chapman, C., Singh, V., 2011. United States Patent. Patent No. US8,014,987B2.
- Paslay, P.R., Bogy, D.B., 1964. The stability of a circular rod laterally constrained to be in contact with an inclined circular cylinder. *J. Appl. Mech. Trans. ASME, Ser. A* 31, 605.
- Senan, N.A.F., O'Reilly, O.M., Treserras, T.N., 2008. Modeling the growth and branching of plants: a simple rod-based model. *J. Mech. Phys. Solids* 56, 3021–3036.
- Su, T., Purohit, P.K., 2011. Entropically driven motion of polymers in non-uniform nanochannels. *Phys. Rev. E* 83, 061906.
- Suryanarayana, P.V.R., McCann, R.C., 1994. Experimental study of buckling and post-buckling of laterally constrained rods. Part I: Frictional effects. In: *Presentation given at ASME Energy-Source Technology Conference and Exhibition, New Orleans, 23–27, January*.
- Suryanarayana, P.V.R., McCann, R.C., 1995. An experiment study of buckling and post-buckling of laterally constrained rod. *ASME J. Energy Resour. Technol.* 117 (2), 115–124.
- Timoshenko, S.P., Gere, J.M., 1961. *Theory of Elastic Stability*, second ed. McGraw-Hill Book Company.
- van der Heijden, G.H.M., Champneys, A.R., Thompson, J.M.T., 2002. Spatially complex localisation in twisted elastic rods constrained to a cylinder. *Int. J. Solids Struct.* 39, 1863–1883.
- Wicks, N., Wardle, B.L., Pafitis, D., 2008. Horizontal cylinder-in-cylinder buckling under compression and torsion: review and application to composite drill pipe. *Int. J. Mech. Sci.* 50, 538–549.
- Wu, C., Li, H., Yu, X., Li, F., Chen, H., Chan, C.T., 2011. Metallic helix array as a broadband wave plate. *Phys. Rev. Lett.* 107, 177401.